COMPARISON BETWEEN DIFFERENT NUMERICAL DISCRETIZATIONS FOR A DARCY-FORCHHEIMER MODEL*

HILDA LÓPEZ†, BRíGIDA MOLINA†, AND JOSÉ J. SALAS‡

Dedicated to Víctor Pereyra on the occasion of his 70th birthday

Abstract. This paper is a numerical study of different discretizations for a mixed formulation of the Darcy-Forchheimer equation. Different finite elements are used: constant functions, conformal linear functions and Crouzeix-Raviart non-conformal finite elements. The behavior of the discretizations is analyzed through a comparative study of some test problems. The numerical results suggest that one of the proposed discretizations has better convergence properties for the velocity.

Key words. Darcy-Forchheimer's model, mixed formulation, numerical discretizations, finite elements, algorithm of alternating directions.

AMS subject classifications. 35Q35, 74S05, 58C15, 65F10

1. Introduction. The following model describes the steady Darcy-Forchheimer flow of a single phase fluid in a porous medium in a bounded domain Ω in two or three dimensions:

$$\frac{\mu}{\rho}K^{-1}\boldsymbol{u} + \frac{\beta}{\rho}|\boldsymbol{u}|\,\boldsymbol{u} + \nabla p = 0 \text{ in } \Omega, \tag{1.1}$$

with the divergence constraint

$$\text{div}\,\boldsymbol{u} = b \text{ in } \Omega, \tag{1.2}$$

and boundary condition

$$\boldsymbol{u}\cdot\boldsymbol{n} = g \text{ on } \partial\Omega, \tag{1.3}$$

where $\boldsymbol{u}$ and p are the velocity vector and the pressure, respectively; $\boldsymbol{n}$ is the unit exterior normal vector to the boundary of Ω; μ, β, and ρ are given positive constants that represent the viscosity of the fluid, its dynamic viscosity, and its density, respectively; $|\cdot|$ denotes the Euclidean norm, $|\boldsymbol{u}|^2 = \boldsymbol{u}\cdot\boldsymbol{u}$; K is the permeability tensor, which is assumed to be uniformly positively defined and bounded; and b and g are given functions that meet the compatibility condition

$$\int_{\Omega} b\,(\boldsymbol{x})\,d\boldsymbol{x} = \int_{\partial\Omega} g\,(\sigma)\,d\sigma.$$

This problem is *nonlinear of monotone type*, and under mild regularity assumptions on the data b and g, it has been demonstrated that a unique weak solution exists; see, for example, [9, 11].

†Centro de Cálculo Científico y Tecnológico, Escuela de Computación, Universidad Central de Venezuela, Caracas, Venezuela. {hlopez,bmolina}@kuaimare.ciens.ucv.ve.
‡Departamento de Educación Física y Matemáticas, Universidad Católica Andrés Bello, Caracas, Venezuela. jsalas@ucab.edu.ve.

From the physical point of view, Darcy's law describes a linear relationship between the velocity vector and the pressure gradient. Experimental evidence shows that when the velocity of the fluid is high enough, a nonlinear relationship is developed between the velocity vector and the pressure gradient, even in the case of a Newtonian flow through a porous medium. Dupuit in 1863 [7] and Forchheimer in 1901 [10] suggested, in the description of this type of flow, modifying Darcy's equation by adding a quadratic term to the velocity with a coefficient that depends on the geometry of the pores. This modification, known as Forchheimer's equation, has led to much research from the experimental [2, 3, 24, 28], theoretical [4, 7, 9, 11], and numerical [16, 17] points of view.

Typically, small velocities are observed in oil reservoirs and aquifers due to the low permeability. In these cases, the nonlinear inertial term becomes insignificant, and we obtain an acceptable approximation for a single flow (mono-phase) through Darcy's law. Nevertheless, there are cases in which the flow velocities are relatively high and the inertial effects cannot be ignored, making Darcy's law inadequate [11].

Also, Rami, Fawzi and Fahmi [14] warn that while Darcy's law is valid for low velocities, and small porosity conditions, in many practical situations, the porous media is bounded by an impermeable wall, near which high flow rates and non-uniform porosity distributions are observed, rendering Darcy's law inapplicable.

The foregoing reasons justify the study of a specific flow in which we consider a nonlinear relationship between the velocity vector and the pressure gradient by means of the Darcy-Forchheimer equation.

Girault and Wheeler [11] demonstrated the existence and uniqueness of a weak solution for the Darcy-Forchheimer problem in the single phase case. In their work, a discretization was studied using mixed finite elements in which the velocity vector and the pressure are approximated by piecewise constants and discontinuous linear functions, respectively; see Crouzeix-Raviart [6]. They also proposed an iterative method of alternating directions of the Peaceman-Rachford type to solve the system of nonlinear equations obtained when the mixed finite elements of Crouzeix-Raviart are applied to Darcy's equation. The convergence of both this iterative method and the mixed finite element method applied to the equation of Darcy-Forchheimer was also demonstrated. Nevertheless, in that work the authors presented only theoretical results without numerical experimentation.

The first objective of this paper is to carry out numerical tests of the methods studied in [11] in order to corroborate the theoretical results presented therein: convergence order $O(h)$ of the finite elements method and convergence properties of the Peaceman-Rachford method. The system of nonlinear equations is also solved by means of Newton's method [13, 15] in order to compare the results with the method proposed in [11].

A second goal is to propose another approximating space of mixed finite elements to calculate low-order approximations using basic and easy-to-implement finite elements. We would also like to have a smoother pressure approximation in comparison to the pressure approximation obtained with the space proposed in [11]. In the space that we propose, the pressure is approximated by continuous functions such that their restriction to each triangle is a polynomial of a degree at most one ($\mathbb{P}_1$). The velocity vector is approximated by constant functions in each triangle. This is one of the spaces presented by Urquiza, Dri, Garon, and Delfour in [26] to solve Darcy's model, and its convergence properties are known for the linear case [22]. To our knowledge, it has never been applied to solve the model of Darcy-Forchheimer.

Finally, since the Peaceman-Rachford method defined in [11] depends on a parameter for decoupling the nonlinearity in (1.1) from the constraint (1.2), a study of the sensitivity of the method with respect to this parameter is presented.

This paper is organized as follows. Section 2 defines the notation used. Section 3 presents some ideas on the weak solution to the problem (1.1)–(1.3) highly developed in [11]. Section 4 discusses the two different mixed finite elements discretizations previously mentioned. Section 5 analyzes the resolution schemes for the discrete problems. The characteristics of each one of the test problems and the numerical results are presented in Section 6. Finally, conclusions and possible extensions are presented in Section 7.

2. Notation. In this section we introduce the Sobolev spaces and the associated norms employed in this paper; see [1, 18] for further details.

Given a domain $\Omega \subset \mathbb{R}^3$ with boundary $\partial\Omega$, let us recall Sobolev's classic space for any non-negative integer m and any number $r \geq 1$:

$$W^{m,r}(\Omega) = \left\{ v \in L^r(\Omega) : \partial^k v \in L^r(\Omega), \forall |k| \leq m \right\},$$

where $|k| = k_1 + k_2 + k_3$, with (k_1, k_2, k_3) a triplet of non negative integers, and the partial derivative ∂^k is

$$\partial^k v = \frac{\partial^{|k|}}{\partial x_1^{k_1} \partial x_2^{k_2} \partial x_3^{k_3}}.$$

This space is equipped with the seminorm

$$|v|_{W^{m,r}(\Omega)} = \left[\sum_{|k|=m} \int_\Omega \left| \partial^k v \right|^r d\boldsymbol{x} \right]^{\frac{1}{r}},$$

and the norm

$$\|v\|_{W^{m,r}(\Omega)} = \left[\sum_{0 \leq k \leq m} \int_\Omega |v|_{W^{k,r}(\Omega)}^r d\boldsymbol{x} \right]^{\frac{1}{r}},$$

with the usual extension in the case $r = \infty$. If $r = 2$, then we obtain the Hilbert space $H^m(\Omega)$. Extensions of this definition to non-integral values of m can be found in [18]. We also use

$$L_0^2(\Omega) = \left\{ \boldsymbol{v} \in L^2(\Omega) : \int_\Omega v(x)dx = 0 \right\}.$$

3. Variational formulation. Some of the ideas developed in [11] on the existence and uniqueness of a weak solution for the equations (1.1)–(1.3) are briefly presented in this section. The following spaces are defined for this purpose:

$$X = L^3(\Omega)^d,$$
$$M = W^{1,\frac{3}{2}}(\Omega) \cap L_0^2(\Omega).$$

The constraints (1.2) and (1.3) are weakened using Green's formula:

$$\int_\Omega \boldsymbol{v} \cdot \nabla q d\boldsymbol{x} = -\int_\Omega q \operatorname{div} \boldsymbol{v} d\boldsymbol{x} + \langle q, \boldsymbol{v} \cdot \mathbf{n} \rangle_{\partial\Omega}, \quad \forall q \in M, \forall \boldsymbol{v} \in H, \qquad (3.1)$$

where

$$H = \left\{ \boldsymbol{v} \in L^3(\Omega)^d : \operatorname{div} \boldsymbol{v} \in L^{\frac{3d}{d+3}}(\Omega) \right\}.$$

Thanks to the validity of (3.1), if we take $b \in L^{\frac{3d}{d+3}}(\Omega)$ and $g \in L^{\frac{3(d-1)}{d}}(\partial\Omega)$, then the problem (1.1)–(1.3) is equivalent to the following variational formulation: find a pair $(\boldsymbol{u}, p)$ in $X \times M$ such that

$$\frac{\mu}{\rho} \int_{\Omega} \left(K^{-1}\boldsymbol{u}\right) \cdot \boldsymbol{\varphi} \, d\boldsymbol{x} + \frac{\beta}{\rho} \int_{\Omega} |\boldsymbol{u}| \left(\boldsymbol{u} \cdot \boldsymbol{\varphi}\right) d\boldsymbol{x} + \int_{\Omega} \nabla p \cdot \boldsymbol{\varphi} d\boldsymbol{x} = 0, \quad \forall \boldsymbol{\varphi} \in X, \quad (3.2)$$

$$\int_{\Omega} \nabla q \cdot \boldsymbol{u} \, d\boldsymbol{x} = -\int_{\Omega} bq \, d\boldsymbol{x} + \int_{\partial\Omega} gq \, d\sigma, \quad \forall q \in M. \quad (3.3)$$

If the given functions b and g satisfy the compatibility condition $\int_{\Omega} b(\boldsymbol{x})d\boldsymbol{x} = \int_{\partial\Omega} g(\sigma)d\sigma$, then this problem has a unique solution $(\boldsymbol{u}, p)$ in $X \times M$; see [11].

4. Discrete variational formulation. Let Ω be a two-dimensional polygon that can be completely triangulated into triangles. Let $\mathcal{T}_h$ be a family of conforming triangulations of $\overline{\Omega}$,

$$\overline{\Omega} = \bigcup_{T \in \mathcal{T}_h} T,$$

which is regular in the sense of Ciarlet [5], i.e., there exists a constant σ independent of h and T such that

$$\forall T \in \mathcal{T}_h, \quad \frac{h_T}{\rho_T} = \sigma_T \leq \sigma,$$

where h_T is the diameter of T and ρ_T the diameter of the sphere inscribed in T. Γ_h denotes the set of all interior edges of triangles in $\mathcal{T}_h$, and b_e is the middle point of an edge $e \in \Gamma_h$.

Using this triangulation $\mathcal{T}_h$ and $\mathbb{P}_k$ (the space of polynomial functions of degree at most k), finite element spaces X_h, M_h are constructed to approximate X and M, respectively. The discrete variational formulation of (3.2)–(3.3) follows: find $(\boldsymbol{u}_h, p_h) \in X_h \times M_h$ such that

$$\frac{\mu}{\rho} \int_{\Omega} \left(K^{-1}\boldsymbol{u}_h\right) \cdot \boldsymbol{\varphi}_h d\boldsymbol{x} + \frac{\beta}{\rho} \int_{\Omega} |\boldsymbol{u}_h| \left(\boldsymbol{u}_h \cdot \boldsymbol{\varphi}_h\right) d\boldsymbol{x}$$
$$+ \sum_{T \in \mathcal{T}_h} \int_T \nabla p_h \cdot \boldsymbol{\varphi}_h d\boldsymbol{x} = 0, \qquad \forall \boldsymbol{\varphi}_h \in X_h, \qquad (4.1)$$

$$\sum_{T \in \mathcal{T}_h} \int_T \nabla q_h \cdot \boldsymbol{u}_h d\boldsymbol{x} = -\int_{\Omega} bq_h d\boldsymbol{x} + \int_{\partial\Omega} gq_h d\sigma, \qquad \forall q_h \in M_h. \qquad (4.2)$$

This discrete problem is a system of nonlinear equations, the numerical solution of which will be studied in Section 5.

Next, the various approximation spaces X_h and M_h used in this paper are described.

4.1. Approximations of velocities by piecewise-constant functions and pressures by Crouzeix-Raviart elements. In this finite element the velocity vector $\boldsymbol{u}$ is approximated by functions from the space

$$X_h^0 = \left\{ \boldsymbol{v} \in L^2(\Omega)^2 : \ \forall T \in \mathcal{T}_h, \boldsymbol{v}|_T \in \mathbb{P}_0^2 \right\}, \qquad (4.3)$$

and the pressure p is approximated by functions from the space

$$M_h^{1,m} = Q_h^{1,m} \cap L_0^2(\Omega), \qquad (4.4)$$

where

$$Q_h^{1,m} = \left\{ q \in L^2(\Omega); \ \forall T \in \mathcal{T}_h, q|_T \in \mathbb{P}_1, \text{ and } \forall e \in \Gamma_h, q \text{ is continuous on } b_e \right\}.$$

The space $Q_h^{1,m}$ is the non-conforming space of degree one introduced and studied by Crouzeix and Raviart in [6]. In [11], the authors demonstrated that the discrete problem (4.1)–(4.2) with the definitions (4.3) and (4.4) has a unique solution. Moreover, if $\mathcal{T}_h$ satisfies (4.1) and the solution $\boldsymbol{u}$ belongs to $W^{1,4}(\Omega)$, then the following error estimations are obtained:

$$\|\boldsymbol{u} - \boldsymbol{u}_h\|_{L^2(\Omega)} \leq Ch\,|\boldsymbol{u}|_{W^{1,4}(\Omega)},$$

$$\left(\sum_{T \in \mathcal{T}_h} \|\nabla(p - p_h)\|_{L^{\frac{3}{2}}(T)}^{\frac{3}{2}}\right)^{\frac{2}{3}} \leq Ch\left(|p|_{W^{2,\frac{3}{2}}(\Omega)} + |\boldsymbol{u}|_{W^{1,4}(\Omega)}\right).$$

The approximation spaces X_h^0 and $Q_h^{1,m}$ are

$$X_h^0 = \operatorname{span}\left\{\begin{bmatrix} v_i \\ 0 \end{bmatrix}, \begin{bmatrix} 0 \\ v_i \end{bmatrix}\right\}, \qquad i = 1, \ldots, N,$$

$$Q_h^{1,m} = \operatorname{span}\{\varphi_i\}, i = 1, \ldots, M,$$

where N is the number of triangles in $\mathcal{T}_h$ and M is the number of edges. The functions v_i are defined as:

$$\forall T_j \in \mathcal{T}_h, \ v_i|_{T_j} = \delta_{ij}, \qquad i, j = 1, \ldots, N,$$

where δ_{ij} the delta of Kronecker. The global basis function φ_i corresponding to node i, which is the middle point of an edge e of the triangulation and its restriction to a triangle T of a global base function φ_i coincides with a local basis function ψ of T. For this finite element, there are three local functions,

$$\psi_1(x, y) = 1 - 2\lambda_1(x, y),$$
$$\psi_2(x, y) = 1 - 2\lambda_2(x, y),$$
$$\psi_3(x, y) = 1 - 2\lambda_3(x, y),$$

where $\lambda_i(x, y)$ is the barycentric coordinate associated to the vertex of triangle T which is in front of edge e_i.

4.2. Approximations of velocities by piecewise-constant functions and pressures by standard finite element $\mathbb{P}_1$. In this case, the space X_h is defined as in (4.3) and the pressures are approximated by functions in the space M_h^1 defined by:

$$M_h^1 = Q_h^1 \cap L_0^2(\Omega), \tag{4.5}$$

where

$$Q_h^1 = \left\{q \in C^0(\overline{\Omega}) : \ \forall T \in \mathcal{T}_h, q|_T \in \mathbb{P}_1\right\}.$$

The space Q_h^1 is a classic continuous finite element space whose nodes are the vertices of the triangles, and the local basis functions are

$$\psi_1(x, y) = \lambda_1(x, y),$$
$$\psi_2(x, y) = \lambda_2(x, y),$$
$$\psi_3(x, y) = 1 - \lambda_1(x, y) - \lambda_2(x, y).$$

It is clear that $X_h^0 \subset X$ and $M_h^1 \subset M$. Then $X_h^0 \times M_h^1$ is a conforming finite element space since it is used as an internal approximation space for $X \times M$.

5. Solution of nonlinear systems. Independent of the discretization used in (4.1)–(4.2), if $\{\varphi_i\}$ is the basis of the approximation space for each of the components of the velocity fields and is $\{\Psi_i\}$ the basis of the approximation space for the pressure, then one can write

$$\boldsymbol{u}_h = \sum_{i=1}^{N} \boldsymbol{u}_h^i \varphi_i \,, \qquad p_h = \sum_{i=1}^{M} p_h^i \Psi_i \,,$$

where $\boldsymbol{u}_h^i$ are the degrees of freedom of the velocity vector and p_h^i the degrees of freedom of the pressure. Then, substituting these expressions into the discrete problem (4.1)–(4.2), we obtain the following equation in "matrix form":

$$\begin{bmatrix} B\left(\widehat{\boldsymbol{u}}\right) & C \\ C^T & 0 \end{bmatrix} \begin{bmatrix} \widehat{\boldsymbol{u}} \\ \widehat{\boldsymbol{p}} \end{bmatrix} = \begin{bmatrix} \boldsymbol{0} \\ \boldsymbol{s} \end{bmatrix}, \tag{5.1}$$

where $\widehat{\boldsymbol{u}} = [\boldsymbol{u}_h^1, \ldots, \boldsymbol{u}_h^N]^T$, $\widehat{p} = [p^1, \ldots, p^M]^T$, $B\left(\widehat{\boldsymbol{u}}\right)\widehat{\boldsymbol{u}}$ is a nonlinear function of $\widehat{\boldsymbol{u}}$ corresponding to

$$\frac{\mu}{\rho}\int_\Omega \left(K_h^{-1}\boldsymbol{u}_h\right)\cdot\boldsymbol{\varphi}_h d\boldsymbol{x} + \frac{\beta}{\rho}\int_\Omega |\boldsymbol{u}_h|\left(\boldsymbol{u}_h\cdot\boldsymbol{\varphi}_h\right)d\boldsymbol{x},$$

C is a matrix corresponding to the term

$$\sum_{T\in\mathcal{T}_h}\int_T \nabla p_h \cdot \varphi_h d\boldsymbol{x},$$

and $\boldsymbol{s}$ represents the right-hand side of (4.2).

In view of the nonlinearity of the problem (5.1), an iterative scheme is required to determine an approximation to the solution of the problem. In this paper, we consider two iterative methods to solve (5.1): an alternating-direction algorithm of the Peaceman-Rachford type proposed in [11] and the classical Newton's method [13, 15]. We briefly describe these methods in the next section.

5.1. Peaceman-Rachford (PR). There are references to Peaceman-Rachford-type methods in the literature on finite differences (see for example [19, 21, 25]) which relate this method to all known Alternating Direction Implicit (ADI) schemes. A good reference for PR-type methods in the solution of linear systems is [29].

In [11] a PR-type algorithm is used for solving (4.1)–(4.2). In that work and for the purpose of decoupling the nonlinearity and the restriction, the authors use the same original idea of the PR method applied to parabolic time dependent problems. Thus, given $\left(\boldsymbol{u}_h^0, p_h^0\right)$, one constructs the sequence $(\boldsymbol{u}_h^n, p_h^n)$ for $n \geq 1$, in two steps:

1. *A nonlinear step without constraints.* Knowing $(\boldsymbol{u}_h^n, p_h^n)$, an intermediate velocity $\boldsymbol{u}_h^{n+\frac{1}{2}}$ is calculated such that:

$$\frac{1}{\alpha}\int_\Omega \left(\boldsymbol{u}_h^{n+\frac{1}{2}} - \boldsymbol{u}_h^n\right)\cdot\boldsymbol{\varphi}_h d\boldsymbol{x} + \frac{\beta}{\rho}\int_\Omega \left|\boldsymbol{u}_h^{n+\frac{1}{2}}\right|\left(\boldsymbol{u}_h^{n+\frac{1}{2}}\cdot\boldsymbol{\varphi}_h\right)d\boldsymbol{x}$$
$$= -\frac{\mu}{\rho}\int_\Omega \left(K^{-1}\boldsymbol{u}_h^n\right)\cdot\boldsymbol{\varphi}_h d\boldsymbol{x} - \sum_T \int_T \nabla p_h^n \cdot \boldsymbol{\varphi}_h d\boldsymbol{x}, \quad \forall\boldsymbol{\varphi}_h \in X_h. \tag{5.2}$$

2. *A linear step with constraints.* Once $\boldsymbol{u}_h^{n+\frac{1}{2}}$ is obtained from the previous step, $\left(\boldsymbol{u}_h^{n+1}, p_h^{n+1}\right)$ is obtained such that:

$$
\frac{1}{\alpha} \int_\Omega \left(\boldsymbol{u}_h^{n+1} - \boldsymbol{u}_h^{n+\frac{1}{2}}\right) \cdot \boldsymbol{\varphi}_h d\boldsymbol{x} + \frac{\mu}{\rho} \int_\Omega \left(K^{-1}\boldsymbol{u}_h^{n+1}\right) \cdot \boldsymbol{\varphi}_h d\boldsymbol{x}
$$

$$
+ \sum_{T \in \mathcal{T}_h} \int_T \nabla p_h^{n+1} \cdot \boldsymbol{\varphi}_h d\boldsymbol{x} = -\frac{\beta}{\rho} \int_\Omega \left|\boldsymbol{u}_h^{n+\frac{1}{2}}\right| \left(\boldsymbol{u}_h^{n+\frac{1}{2}} \cdot \boldsymbol{\varphi}_h\right) d\boldsymbol{x}, \qquad \forall \boldsymbol{\varphi}_h \in X_h, \qquad (5.3)
$$

$$
\sum_{T \in \mathcal{T}_h} \int_T \nabla q_h \cdot u_h^{n+1} d\boldsymbol{x} = -\int_\Omega b q_h d\boldsymbol{x} + \int_{\partial\Omega} g q_h d\sigma, \qquad \forall q_h \in M_h, \qquad (5.4)
$$

where α is a positive parameter.

Since the equation (1.1) differs from Darcy's equation in the nonlinear term $\frac{\beta}{\rho}|\boldsymbol{u}|\boldsymbol{u}$, a natural way to select the initial guess $\left(\boldsymbol{u}_h^0, p_h^0\right)$ is by solving a linear Darcy step:

$$
\frac{\mu}{\rho} \int_\Omega \left(K^{-1}\boldsymbol{u}_h^0\right) \cdot \boldsymbol{\varphi}_h d\boldsymbol{x} + \sum_{T \in \mathcal{T}_h} \int_T \nabla p_h^0 \cdot \boldsymbol{\varphi}_h d\boldsymbol{x} = 0, \qquad \forall \boldsymbol{\varphi}_h \in X_h, \qquad (5.5)
$$

$$
\sum_{T \in \mathcal{T}_h} \int_T \nabla q_h \cdot \boldsymbol{u}_h^0 d\boldsymbol{x} = -\int_\Omega b q_h d\boldsymbol{x} + \int_{\partial\Omega} g q_h d\sigma, \qquad \forall q_h \in M_h. \qquad (5.6)
$$

Problems (5.3)–(5.4) and (5.5)–(5.6) are written in matrix form as

$$
M\boldsymbol{y} = \boldsymbol{z}, \qquad (5.7)
$$

where the matrix of coefficients M has a block structure

$$
M = \begin{bmatrix} X & C \\ C^T & 0 \end{bmatrix} \quad \text{and} \quad \boldsymbol{z} = \begin{bmatrix} \boldsymbol{r} & \boldsymbol{s} \end{bmatrix}^T.
$$

Then, for the problem (5.3)–(5.4), $X = A + \frac{1}{\alpha}I$ with A the symmetric matrix associated to the term $\frac{\mu}{\rho} \int_\Omega \left(K^{-1}\boldsymbol{u}_h^{n+1}\right) \cdot \boldsymbol{\varphi}_h d\boldsymbol{x}$ and $\boldsymbol{r}$ represents the right-hand side of (5.3). For the problem (5.5)–(5.6), $X = A$ and $\boldsymbol{z} = \begin{bmatrix} \boldsymbol{0} & \boldsymbol{s} \end{bmatrix}^T$. Considering the characteristics of the coefficient matrix M, both linear systems were solved with MINRES.

In [11], the authors demonstrate that the problems (4.1)–(4.2) and (5.5)–(5.6) have a unique solution for the finite element spaces (4.3) and (4.4), and that the iterative method defined by (5.2)–(5.4) is convergent for an arbitrary choice of the initial approximation $\left(\boldsymbol{u}_h^0, p_h^0\right)$ and any $\alpha > 0$.

Curiously, the solution to the problem (5.2) can be calculated explicitly for the finite element spaces (4.3) and (4.4). This is also true for the finite element spaces considered in the second discretization (4.3) and (4.5), since the space that approximates the velocities has not changed. Thus, in each iteration, the solution of (5.2) is explicitly calculated and then this solution is introduced in (5.3)–(5.4), leading to a linear system of the form given in (5.7).

The explicit solution of (5.2) is calculated as follows. The space X_h^0 consists of constant functions on each triangle T; hence, the test functions $\boldsymbol{\varphi}_h$, as well as the solution $\boldsymbol{u}_h^{n+\frac{1}{2}}$ and ∇p_h^n are constants on each element T. Therefore, a quick calculation leads to:

$$
\boldsymbol{u}_T^{n+\frac{1}{2}} = \frac{1}{\gamma} F_T^{n+\frac{1}{2}},
$$

where $\quad F_T^{n+\frac{1}{2}} = \frac{1}{\alpha}\boldsymbol{u}_T^n - \frac{\mu}{\rho}K_T^{-1}\boldsymbol{u}_T^n - \nabla_T p_h^n, \quad \gamma = \frac{1}{2\alpha} + \frac{1}{2}\sqrt{\frac{1}{\alpha^2} + 4\frac{\beta}{\rho}\left|F_T^{n+\frac{1}{2}}\right|}$, and $K_T^{-1} = \frac{1}{|T|}\int_T K^{-1}(x)\,dx$. For further details, see [11].

5.2. Newton's method. For discretizations $X_h^0 \times M_h^1$ and $X_h^0 \times M_h^{1,m}$, let us recall that X_h and M_h are made up of functions from $\mathbb{P}_0$ and $\mathbb{P}_1$, respectively, over each $T \in \mathcal{T}_h$. Therefore, the basis functions of X_h and the gradient of the basis functions of M_h are constants over each T. Hence, the nonlinear problem (4.1)–(4.2) is written as

$$G\left(\boldsymbol{w}\right) = \begin{bmatrix} \mathbf{0} \\ \boldsymbol{s} \end{bmatrix} \quad \text{with} \quad \boldsymbol{w} = [u_x^1, u_y^1, \ldots, u_x^N, u_y^N, p^1, \ldots, p^M]^T,$$

where

$$G\left(\boldsymbol{w}\right) = \begin{bmatrix} A_{T_i} (\frac{\mu}{\rho} K_{T_i}^{-1} \boldsymbol{u}^i + \frac{\beta}{\rho} |\boldsymbol{u}^i| \boldsymbol{u}^i + \sum_{j=1}^{3} p^{i_j} \nabla \psi_{i_j}) \\ \sum_{T_i \in Supp(\Psi_j)} A_{T_i} \nabla \Psi_j \cdot \boldsymbol{u}^i \end{bmatrix}_{i=1,\ldots N, \ j=1,\ldots,M}. \quad (5.8)$$

Here A_{T_i} is the area of triangle T_i; ψ_{i_j}, $j = 1, 2, 3$, are the restrictions of the basis functions associated to the midpoints of the edges of the triangle T_i; and p^{i_j}, $j = 1, 2, 3$, are the degrees of freedom of the pressure associated to the midpoints of the edges of triangle T_i. Thus, Newton's method is written as:

$$\boldsymbol{w}_0 \text{ given}$$
$$\text{for } k = 0, 1, \ldots,$$
$$DG(\boldsymbol{w}_k)\boldsymbol{\varepsilon}_k = -G(\boldsymbol{w}_k) + \begin{bmatrix} \mathbf{0} & \boldsymbol{s} \end{bmatrix}^T,$$
$$\boldsymbol{w}_{k+1} = \boldsymbol{w}_k + \boldsymbol{\varepsilon}_k,$$

where $DG(\boldsymbol{w}_k)$ is the Jacobian matrix with respect to $\boldsymbol{u}^i, p^j, i = 1, \ldots, N, j = 1, \ldots, M$. This Jacobian matrix has the same structure as matrix M and it is symmetric, since the upper left block is A plus the Jacobian of the nonlinear term $\frac{\beta}{\rho} |\boldsymbol{u}| \boldsymbol{u}$, which is symmetric, and the other blocks are the same blocks as in the matrix M.

In each Newton step, the Jacobian matrix is computed explicitly. Since the linear system in Newton's method and those that appear in (5.3)–(5.4) and (5.5)–(5.6) are symmetric, we use MINRES [12, 20, 23, 27] to solve them.

6. Numerical Results. In this section, we present results of numerical experiments that were designed to test the effectiveness of the PR method compared with Newton's method, considering two different discretizations of the variational formulation of the Darcy-Forchheimer problem (4.1)–(4.2). The numerical experimentation was accomplished through three test problems of the form:

$$\frac{\mu}{\rho} K^{-1} \boldsymbol{u} + \frac{\beta}{\rho} |\boldsymbol{u}| \boldsymbol{u} + \nabla p = \boldsymbol{f}(x, y) \text{ in } \Omega,$$
$$\text{div } \boldsymbol{u} = b \text{ in } \Omega,$$
$$\boldsymbol{u} \cdot \boldsymbol{n} = g \text{ on } \partial \Omega,$$

where $\Omega \subset \mathbb{R}^2$ is a square defined as:

$$\Omega = \{(x, y) \in \mathbb{R}^2 : \ -1 < x < 1, \ -1 < y < 1\}.$$

The first test problem is defined as follows:

$$\boldsymbol{f}\left(x, y\right) = \begin{bmatrix} \left(1 + \beta\sqrt{2x^2 + 2y^2}\right)(x + y) + 3x^2 \\ \left(1 + \beta\sqrt{2x^2 + 2y^2}\right)(x - y) + 3y^2 \end{bmatrix}$$

and

$$
g\left(x, y\right) = \begin{cases} 1 + y, & x = 1, \\ 1 - y, & x = -1, \\ x - 1, & y = 1, \\ -x - 1, & y = -1, \end{cases}
$$

so that the exact velocity field and the pressure function are

$$
\boldsymbol{u}\left(x, y\right) = \left(x + y, x - y\right)^T, \qquad p(x, y) = x^3 + y^3.
$$

For the second test problem, we use

$$
\boldsymbol{f}\left(x, y\right) = \begin{bmatrix} \frac{(x+1)^2}{4}\left(1 + \beta\frac{(x+1)}{4}\sqrt{(x+1)^2 + 4\left(y+1\right)^2}\right) + 3x^2 \\ -\frac{(x+1)(y+1)}{2}\left(1 + \beta\frac{(x+1)}{4}\sqrt{(x+1)^2 + 4\left(y+1\right)^2}\right) + 3y^2 \end{bmatrix},
$$

and

$$
g\left(x, y\right) = \begin{cases} 1, & x = 1, \\ 0, & x = -1, \\ -(x+1), & y = 1, \\ 0, & y = -1, \end{cases}
$$

Here, the exact velocity field and the pressure function are

$$
\boldsymbol{u}\left(x, y\right) = \left(\frac{(x+1)^2}{4}, -\frac{(x+1)(y+1)}{2}\right)^T, \qquad p(x, y) = x^3 + y^3.
$$

Finally, for the third test problem, we selected

$$
\boldsymbol{f}\left(x, y\right) = \begin{bmatrix} 2y(1 - x^2)\left(1 + 2\beta\sqrt{y^2(1 - x^2)^2 + x^2(1 - y^2)^2}\right) + 3x^2 \\ -2x(1 - y^2)\left(1 + 2\beta\sqrt{y^2(1 - x^2)^2 + x^2(1 - y^2)^2}\right) + 3y^2 \end{bmatrix}
$$

and

$$
g(x, y) = 0 \text{ on } \partial\Omega.
$$

In this case, the exact solution of the velocity field and the corresponding pressure function are

$$
\boldsymbol{u}\left(x, y\right) = \left(2y(1 - x^2), -2x(1 - y^2)\right)^T, \qquad p(x, y) = x^3 + y^3.
$$

The last two problems were taken from [26].

For all the problems, μ and ρ were taken to be 1 and $K = I_{2\times2}$. Numerical tests were carried out using different values for parameter β in order to study the behavior of the methods as the nonlinearity of the problem increases.

We use a classical triangulation $\mathcal{T}_h$ built with a family of three parallel lines, meaning that the square Ω is divided into $L \times L$ squares of a size h with $L = 2/h$, which are divided
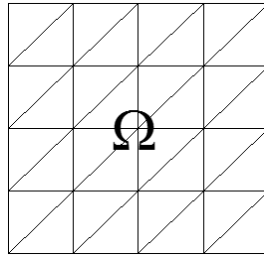
FIGURE 6.1. *Triangulation $\mathcal{T}_h$ with $h = 1/2$.*

into two rectangular triangles by tracing the ascending diagonal line. Figure 6.1 shows this type of triangulation.

It is easy to verify that the size of the vector velocity approximation is $4L^2$ for both mixed finite elements spaces, $X_h^0 \times M_h^{1,m}$ and $X_h^0 \times M_h^1$. The size of the vector pressure approximation is $L(3L + 2)$ and $(L + 1)^2$ for $M_h^{1,m}$ and M_h^1, respectively.

All the experiments were run on a Intel Core 2 Duo E4300, 1.8 GHz using MATLAB 7.0. For the two approximation spaces considered, the calculations were made for different values of h: $1/8$, $1/16$, and $1/32$. The exact solution is known in all the cases and the stopping criterion was:

$$e_n = \|\boldsymbol{u} - \boldsymbol{u}_h^n\|_{L^2(\Omega)} \le tol,$$

where tol is a given parameter. In the experiments tol was set to $1.95h$, except in the third experiment. A maximum of 2100 iterations was enough to reach convergence in all cases.

In order to make an adequate comparison, the initial guess for Newton's method and the PR method were the same. Although there is no proof of convergence for Newton's method with this initial guess, in all cases the method successfully converged. The stopping criterion for MINRES was 10^{-12} in the 2-norm of the residual.

As we mentioned previously, the PR method with $X_h^0 \times M_h^{1,m}$ converges for any $\alpha > 0$. Nevertheless, in practice, it could be observed that its behavior is very sensitive to the choice of this parameter. For this reason it is very important to select an appropriate value.

In our first experiment, we conducted a comparative study of the PR algorithm for different choices of the parameter α. Numerical tests were performed for all the problems and the two discretizations defined in the previous section. The behavior of the algorithm with respect to the parameter α was similar for all the problems and for both discretizations. Thus, we only report graphs showing a comparative study of the parameter α for problem 3 when $\beta = 50$ and $h = 1/8$.

Figures 6.2(a) and 6.2(b) report the behavior of the algorithm with respect to the number of iterations for six values of α in the interval $(0, 1]$ and for discretizations $X_h^0 \times M_h^1$ and $X_h^0 \times M_h^{1,m}$, respectively, while Figures 6.3(a) and 6.3(b) show the behavior of the algorithm for six different values of α in the interval $[1, 150]$ and for discretizations $X_h^0 \times M_h^1$ and $X_h^0 \times M_h^{1,m}$, respectively. It can be observed that, regardless of the discretization, the best results were obtained when $\alpha = 1$, $\alpha = 0.01$, and $\alpha = 5$, whereas the worst results were achieved when α was too close to zero or greater than 50. This led us to study the spectrum of the coefficients matrix M in the PR method. It was observed that, for both discretization spaces, for α values near zero or greater than 50, that the minimum eigenvalue of M tends to zero and the condition number increases, influencing the rate of convergence of MINRES. This study confirms our numerical results with respect to the choice of the α value.
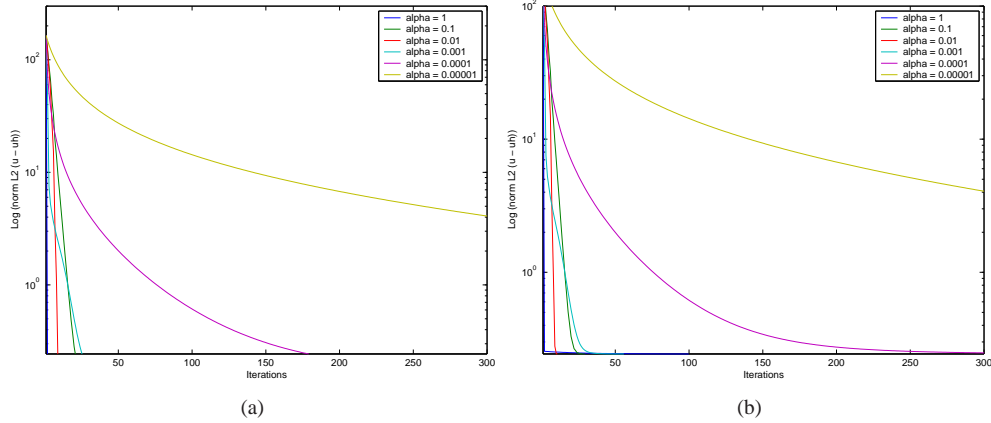
FIGURE 6.2. *(a) Problem 3 with $\beta = 50$, $\alpha \in (0,1]$ and discretization $X_h^0 \times M_h^1$. (b) Problem 3 with $\beta = 50$, $\alpha \in (0,1]$ and discretization $X_h^0 \times M_h^{1,m}$.*
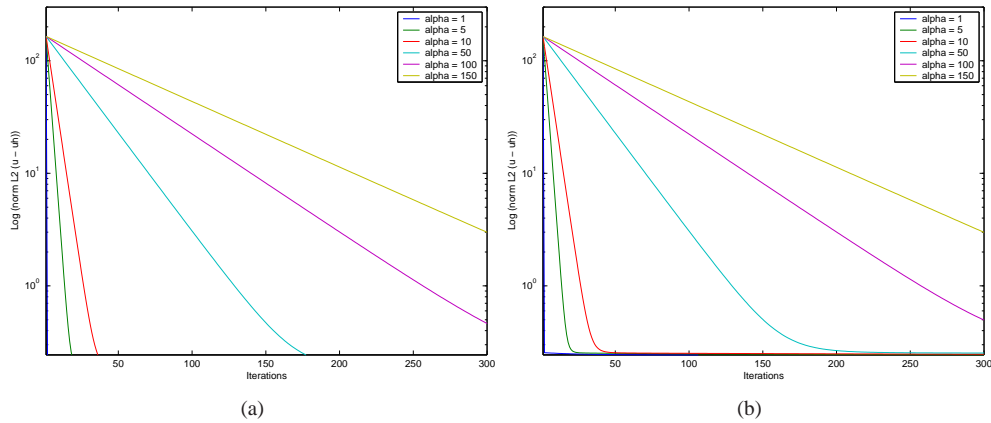

FIGURE 6.3. *(a) Problem 3 with $\beta = 50$, $\alpha \in [1,150]$ and discretization $X_h^0 \times M_h^1$. (b) Problem 3 with $\beta = 50$, $\alpha \in [1,150]$ and discretization $X_h^0 \times M_h^{1,m}$.*

Based on all the numerical tests conducted, it was determined that the best results, in most cases, were achieved for $\alpha = 1$; therefore, this value of α is used in the PR algorithm in the remaining experiments.

In the second experiment, we study the behavior of the Peaceman-Rachford algorithm with the two discretizations considered in this paper for the three test problems. Different values of the discretization parameter h and several values of the parameter β were considered. Tables 6.1, 6.2, and 6.3 report the number of iterations and the error of the velocity vector in the $L^2(\Omega)$ norm.

We observe that for different values of β, the number of iterations required by PR is similar in both discretizations. However, the computational cost of solving the linear system for the discretization $X_h^0 \times M_h^{1,m}$ is higher, since the size of the system for this discretization is approximately, 30% bigger. Therefore, we conclude that the discretization using $X_h^0 \times M_h^1$ is more attractive for this method.

The third experiment tries to establish the order of convergence of the discretizations considered in this paper. In this experiment, tol was set to $0.95h$ to demand higher accuracy

TABLE 6.1
Comparison between $X_h^0 \times M_h^{1,m}$ and $X_h^0 \times M_h^1$ discretizations of Problem 1 (using PR).

β		$iter$	$h=\frac{1}{8}$ $\|\mathbf{u}-\mathbf{u}_h\|_{L^2(\Omega)}$	$iter$	$h=\frac{1}{16}$ $\|\mathbf{u}-\mathbf{u}_h\|_{L^2(\Omega)}$	$iter$	$h=\frac{1}{32}$ $\|\mathbf{u}-\mathbf{u}_h\|_{L^2(\Omega)}$
10	$X_h^0 \times M_h^{1,m}$	7	0.2399	13	0.1161	19	0.0602
	$X_h^0 \times M_h^1$	7	0.2210	11	0.1154	17	0.0585
20	$X_h^0 \times M_h^{1,m}$	13	0.2400	24	0.1190	37	0.0602
	$X_h^0 \times M_h^1$	12	0.2375	20	0.1210	32	0.0607
30	$X_h^0 \times M_h^{1,m}$	19	0.2401	35	0.1201	55	0.0602
	$X_h^0 \times M_h^1$	18	0.2330	30	0.1192	48	0.0600
40	$X_h^0 \times M_h^{1,m}$	25	0.2401	46	0.1207	72	0.0609
	$X_h^0 \times M_h^1$	23	0.2389	39	0.1212	63	0.0608
50	$X_h^0 \times M_h^{1,m}$	31	0.2402	57	0.1210	90	0.0608
	$X_h^0 \times M_h^1$	28	0.2427	49	0.1201	79	0.0603

TABLE 6.2
Comparison between $X_h^0 \times M_h^{1,m}$ and $X_h^0 \times M_h^1$ discretizations of Problem 2 (using PR).

β		$iter$	$h=\frac{1}{8}$ $\|\mathbf{u}-\mathbf{u}_h\|_{L^2(\Omega)}$	$iter$	$h=\frac{1}{16}$ $\|\mathbf{u}-\mathbf{u}_h\|_{L^2(\Omega)}$	$iter$	$h=\frac{1}{32}$ $\|\mathbf{u}-\mathbf{u}_h\|_{L^2(\Omega)}$
10	$X_h^0 \times M_h^{1,m}$	10	0.2282	15	0.1204	22	0.0589
	$X_h^0 \times M_h^1$	10	0.2201	15	0.1181	22	0.0582
20	$X_h^0 \times M_h^{1,m}$	19	0.2336	30	0.1180	43	0.0604
	$X_h^0 \times M_h^1$	18	0.2346	29	0.1183	42	0.0607
30	$X_h^0 \times M_h^{1,m}$	28	0.2360	44	0.1210	65	0.0596
	$X_h^0 \times M_h^1$	26	0.2407	43	0.1186	63	0.0602
40	$X_h^0 \times M_h^{1,m}$	37	0.2372	59	0.1200	86	0.0604
	$X_h^0 \times M_h^1$	35	0.2363	57	0.1189	84	0.0599
50	$X_h^0 \times M_h^{1,m}$	45	0.2433	73	0.1216	108	0.0601
	$X_h^0 \times M_h^1$	43	0.2399	70	0.1216	104	0.0609

and to observe the convergence order. The experimental results corroborate the $O(h)$ convergence for the velocity vector approximation that was predicted in [11] for the discretization space $X_h^0 \times M_h^{1,m}$. The experiments also indicate that the convergence for the velocity vector approximation is $O(h)$ for the discretization space $X_h^0 \times M_h^1$. Tables 6.4 and 6.5 show these results for problem 2 when $h = 1/8$, $h = 1/16$, $h = 1/32$, and $h = 1/64$.

In all the numerical tests, the stopping criterion was $\|\boldsymbol{u} - \boldsymbol{u}_h^n\|_{L^2(\Omega)} \le tol$ without taking into account the pressure accuracy. Tables 6.6 and 6.7 show the error $\|p - p_h\|_{H^1(\Omega)}$ corresponding to the results shown in Tables 6.4 and 6.5, respectively. It is clear that the accuracy of the pressure approximations is very bad. Nevertheless, it is worth noting that the experimental convergence order is $O(h)$.

In view of these results, we would like to study how many iterations would be necessary to achieve an error in the pressure approximation similar to the one which is being demanded from the velocity vector. Tables 6.8 and 6.9 show the error $\|p - p_h\|_{H^1(\Omega)}$ for pressure approximations obtained with 300 iterations. We can see from these tables that the accuracy of the pressure is far from satisfying the velocity vector's accuracy in all cases, i.e., for different values of the discretization parameter h and the different values of parameter β. Therefore, this method seems to be very computationally expensive to obtain a good approximation of the pressure.

The fourth and last experiment compares the PR method with the well-known Newton method for solving nonlinear systems. Tables 6.10, 6.11, and 6.12 show the results for Newton's method using the discretizations $X_h^0 \times M_h^{1,m}$ and $X_h^0 \times M_h^1$.

TABLE 6.3
Comparison between $X_h^0 \times M_h^{1,m}$ and $X_h^0 \times M_h^1$ discretizations of Problem 3 (using PR).

β		$h = \frac{1}{8}$		$h = \frac{1}{16}$		$h = \frac{1}{32}$	
		iter	$\|\mathbf{u} - \mathbf{u}_h\|_{L^2(\Omega)}$	*iter*	$\|\mathbf{u} - \mathbf{u}_h\|_{L^2(\Omega)}$	*iter*	$\|\mathbf{u} - \mathbf{u}_h\|_{L^2(\Omega)}$
10	$X_h^0 \times M_h^{1,m}$	17	0.2437	27	0.1219	36	0.0609
	$X_h^0 \times M_h^1$	2	0.1806	2	0.1102	8	0.0585
20	$X_h^0 \times M_h^{1,m}$	32	0.2437	54	0.1219	71	0.0609
	$X_h^0 \times M_h^1$	2	0.1822	2	0.1130	14	0.0602
30	$X_h^0 \times M_h^{1,m}$	48	0.2437	80	0.1219	106	0.0609
	$X_h^0 \times M_h^1$	2	0.1828	2	0.1140	20	0.0608
40	$X_h^0 \times M_h^{1,m}$	64	0.2437	106	0.1219	140	0.0609
	$X_h^0 \times M_h^1$	2	0.1831	2	0.1146	27	0.0604
50	$X_h^0 \times M_h^{1,m}$	80	0.2437	132	0.1219	175	0.0609
	$X_h^0 \times M_h^1$	2	0.1833	2	0.1149	33	0.0607

TABLE 6.4
L^2 error in the velocity vector for $X_h^0 \times M_h^1$ of Problem 2 (using PR).

β		$h = \frac{1}{8}$		$h = \frac{1}{16}$		$h = \frac{1}{32}$		$h = \frac{1}{64}$
	iter	$\|\mathbf{u} - \mathbf{u}_h\|_{L^2(\Omega)}$	*iter*	$\|\mathbf{u} - \mathbf{u}_h\|_{L^2(\Omega)}$	*iter*	$\|\mathbf{u} - \mathbf{u}_h\|_{L^2(\Omega)}$	*iter*	$\|\mathbf{u} - \mathbf{u}_h\|_{L^2(\Omega)}$
10	19	0.115777	27	0.058054	35	0.029657	45	0.014556
20	34	0.116988	49	0.058556	65	0.029663	83	0.014772
30	49	0.118094	71	0.059097	96	0.029348	122	0.014767
40	65	0.117002	94	0.058702	126	0.029548	161	0.014785
50	80	0.117932	116	0.059148	157	0.029409	200	0.014809

TABLE 6.5
L^2 error in the velocity vector for $X_h^0 \times M_h^{1,m}$ of Problem 2 (using PR).

β		$h = \frac{1}{8}$		$h = \frac{1}{16}$		$h = \frac{1}{32}$		$h = \frac{1}{64}$
	iter	$\|\mathbf{u} - \mathbf{u}_h\|_{L^2(\Omega)}$	*iter*	$\|\mathbf{u} - \mathbf{u}_h\|_{L^2(\Omega)}$	*iter*	$\|\mathbf{u} - \mathbf{u}_h\|_{L^2(\Omega)}$	*iter*	$\|\mathbf{u} - \mathbf{u}_h\|_{L^2(\Omega)}$
10	23	0.1180	30	0.0593	39	0.0293	48	0.0146
20	46	0.1180	60	0.0592	76	0.0297	94	0.0148
30	69	0.1182	90	0.0593	115	0.0295	141	0.0148
40	92	0.1183	121	0.0592	153	0.0296	188	0.0148
50	115	0.1185	151	0.0593	191	0.0297	236	0.0148

TABLE 6.6
H^1-error in the pressure for $X_h^0 \times M_h^1$ of Problem 2 (using PR).

β	$h = \frac{1}{8}$	$h = \frac{1}{16}$	$h = \frac{1}{32}$	$h = \frac{1}{64}$
	$\|p - p_h\|_{H^1(\Omega)}$	$\|p - p_h\|_{H^1(\Omega)}$	$\|p - p_h\|_{H^1(\Omega)}$	$\|p - p_h\|_{H^1(\Omega)}$
10	3.2904	1.8173	1.0408	0.5384
20	7.3398	4.1593	2.3604	1.2929
30	11.4311	6.5330	3.6103	2.0186
40	15.2159	8.7497	4.9460	2.7460
50	19.3172	11.1320	6.1974	3.4741

In all problems and for different values of β, if the discretization parameter h decreases, then more steps were required for the discretization $X_h^0 \times M_h^{1,m}$ than for the discretization $X_h^0 \times M_h^1$. This behavior was more pronounced for problems 1 and 3.

On the other hand, if the results obtained in Tables 6.1–6.3 and 6.10–6.12 are compared, it can be observed that in all experiments, the PR algorithm required fewer iterations than Newton's method. Figures 6.4, 6.5, and 6.6 show this behavior for the three test problems when $\beta = 20$ and $h = 1/32$. It is also worthwhile mentioning that the computer cost

TABLE 6.7
H^1-error in the pressure for $X_h^0 \times M_h^{1,m}$ of Problem 2 (using PR).

β	$h = \frac{1}{8}$ $\|p - p_h\|_{H^1(\Omega)}$	$h = \frac{1}{16}$ $\|p - p_h\|_{H^1(\Omega)}$	$h = \frac{1}{32}$ $\|p - p_h\|_{H^1(\Omega)}$	$h = \frac{1}{64}$ $\|p - p_h\|_{H^1(\Omega)}$
10	2.6589	1.5737	0.8486	0.4698
20	5.0690	3.0083	1.7230	0.9531
30	7.4851	4.4454	2.4983	1.4099
40	9.9030	5.7956	3.3234	1.8668
50	12.3214	7.2339	4.1485	2.2973

TABLE 6.8
H^1 error in the pressure for $X_h^0 \times M_h^1$ of Problem 2 with 300 iterations (using PR).

β	$h = \frac{1}{8}$ $\|p - p_h\|_{H^1(\Omega)}$	$h = \frac{1}{16}$ $\|p - p_h\|_{H^1(\Omega)}$	$h = \frac{1}{32}$ $\|p - p_h\|_{H^1(\Omega)}$	$h = \frac{1}{64}$ $\|p - p_h\|_{H^1(\Omega)}$
10	0.3553	0.1772	0.0885	0.0442
20	0.3559	0.1773	0.0885	0.0443
30	0.3629	0.1865	0.1052	0.0721
40	0.4719	0.3586	0.3271	0.3192
50	0.9871	0.9663	0.9649	0.9652

TABLE 6.9
H^1 error for the pressure for $X_h^0 \times M_h^{1,m}$ of Problem 2 with 300 iterations (using PR).

β	$h = \frac{1}{8}$ $\|p - p_h\|_{H^1(\Omega)}$	$h = \frac{1}{16}$ $\|p - p_h\|_{H^1(\Omega)}$	$h = \frac{1}{32}$ $\|p - p_h\|_{H^1(\Omega)}$	$h = \frac{1}{64}$ $\|p - p_h\|_{H^1(\Omega)}$
10	1.2886	0.6441	0.3220	0.1610
20	2.4543	1.2272	0.6135	0.3068
30	3.6227	1.8119	0.9072	0.4562
40	4.7741	2.4019	1.2314	0.6739
50	5.9343	3.0806	1.7518	1.2106

TABLE 6.10
Comparison between $X_h^0 \times M_h^{1,m}$ and $X_h^0 \times M_h^1$ discretizations of Problem 1 (using Newton).

β		$h = \frac{1}{8}$ $iter$	$\|\mathbf{u} - \mathbf{u}_h\|_{L^2(\Omega)}$	$h = \frac{1}{16}$ $iter$	$\|\mathbf{u} - \mathbf{u}_h\|_{L^2(\Omega)}$	$h = \frac{1}{32}$ $iter$	$\|\mathbf{u} - \mathbf{u}_h\|_{L^2(\Omega)}$
10	$X_h^0 \times M_h^{1,m}$	29	0.2416	83	0.1207	430	0.0609
	$X_h^0 \times M_h^1$	8	0.2369	26	0.1210	83	0.0597
20	$X_h^0 \times M_h^{1,m}$	52	0.2419	203	0.1218	608	0.0609
	$X_h^0 \times M_h^1$	19	0.2319	49	0.1201	154	0.0601
30	$X_h^0 \times M_h^{1,m}$	89	0.2410	322	0.1217	895	0.0609
	$X_h^0 \times M_h^1$	30	0.2419	79	0.1192	249	0.0607
40	$X_h^0 \times M_h^{1,m}$	146	0.2427	471	0.1213	1305	0.0608
	$X_h^0 \times M_h^1$	47	0.2346	118	0.1218	321	0.0605
50	$X_h^0 \times M_h^{1,m}$	205	0.2436	629	0.1218	1664	0.0609
	$X_h^0 \times M_h^1$	58	0.2415	159	0.1207	410	0.0606

for Newton is higher than for PR iteration, because in each iteration, Newton evaluates the Jacobian and solves a system of linear equations, and PR solves a linear system of equations and calculates an intermediate solution. The computer cost of this calculation is negligible in comparison with the Jacobian evaluation. For these reasons, the PR algorithm is much more attractive.

7. Conclusions. This paper presents a comparative study between the Peaceman-Rachford iterative method and Newton's method with two different discretizations of a flow using

TABLE 6.11
Comparison between $X_h^0 \times M_h^{1,m}$ and $X_h^0 \times M_h^1$ discretizations of Problem 2 (using Newton).

β			$h = \frac{1}{8}$		$h = \frac{1}{16}$		$h = \frac{1}{32}$
		$iter$	$\|\mathbf{u} - \mathbf{u}_h\|_{L^2(\Omega)}$	$iter$	$\|\mathbf{u} - \mathbf{u}_h\|_{L^2(\Omega)}$	$iter$	$\|\mathbf{u} - \mathbf{u}_h\|_{L^2(\Omega)}$
10	$X_h^0 \times M_h^{1,m}$	39	0.2431	110	0.1182	427	0.0609
	$X_h^0 \times M_h^1$	12	0.2362	35	0.1186	103	0.0601
20	$X_h^0 \times M_h^{1,m}$	77	0.2380	240	0.1207	760	0.0609
	$X_h^0 \times M_h^1$	27	0.2424	66	0.1207	196	0.0607
30	$X_h^0 \times M_h^{1,m}$	141	0.2423	415	0.1212	1189	0.0609
	$X_h^0 \times M_h^1$	39	0.2437	99	0.1198	311	0.0606
40	$X_h^0 \times M_h^{1,m}$	139	0.2428	560	0.1214	1563	0.0608
	$X_h^0 \times M_h^1$	59	0.2349	153	0.1210	413	0.0594
50	$X_h^0 \times M_h^{1,m}$	191	0.2433	768	0.1218	2008	0.0609
	$X_h^0 \times M_h^1$	75	0.2396	203	0.1197	531	0.0608

TABLE 6.12
Comparison between $X_h^0 \times M_h^{1,m}$ and $X_h^0 \times M_h^1$ discretizations of Problem 3 (using Newton).

| β			$h = \frac{1}{8}$		$h = \frac{1}{16}$		$h = \frac{1}{32}$
		$iter$	$\|\mathbf{u} - \mathbf{u}_h\|_{L^2(\Omega)}$	$iter$	$\|\mathbf{u} - \mathbf{u}_h\|_{L^2(\Omega)}$	$iter$	$\|\mathbf{u} - \mathbf{u}_h\|_{L^2(\Omega)}$
10	$X_h^0 \times M_h^{1,m}$	12	0.2437	42	0.1219	116	0.0609
	$X_h^0 \times M_h^1$	6	0.1910	7	0.1108	16	0.0562
20	$X_h^0 \times M_h^{1,m}$	19	0.2437	90	0.1219	371	0.0609
	$X_h^0 \times M_h^1$	7	0.2071	9	0.1082	22	0.0592
30	$X_h^0 \times M_h^{1,m}$	27	0.2435	136	0.1219	426	0.0609
	$X_h^0 \times M_h^1$	8	0.1901	11	0.1107	28	0.0594
40	$X_h^0 \times M_h^{1,m}$	35	0.2437	170	0.1219	589	0.0609
	$X_h^0 \times M_h^1$	8	0.2365	13	0.1217	39	0.0605
50	$X_h^0 \times M_h^{1,m}$	42	0.2437	225	0.1219	791	0.0609
	$X_h^0 \times M_h^1$	9	0.2052	16	0.1184	48	0.0599
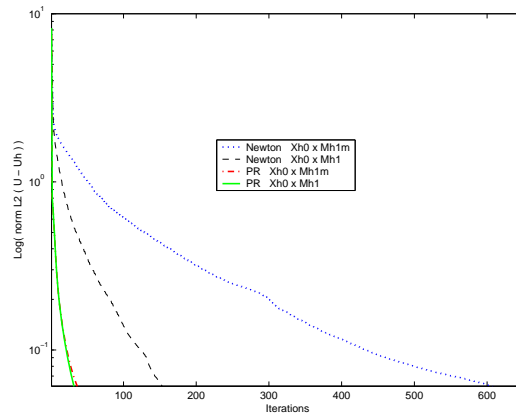
FIGURE 6.4. *Number of iterations vs absolute error in the solution of Problem 1 using $X_h^0 \times M_h^{1,m}$ and $X_h^0 \times M_h^1$ discretizations and the methods PR and Newton.*

Darcy-Forchheimer's equation. Newton's method is not competitive with the PR method, because the PR method has a lower cost per iteration and requires fewer iterations to achieve convergence. The parameter α in the PR method was set to its best value after some experiments. The convergence order for the discretization $X_h^0 \times M_h^1$ with PR was determined experimentally, and the convergence order for the discretization $X_h^0 \times M_h^{1,m}$, determined the-
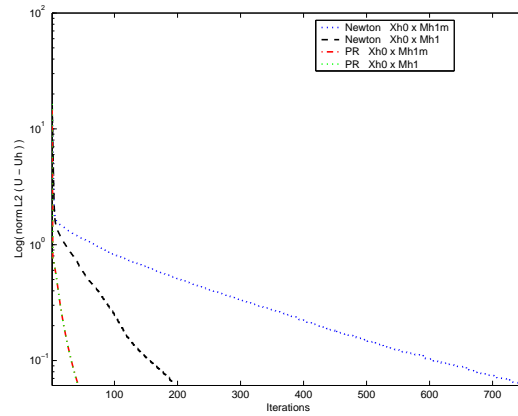
FIGURE 6.5. *Number of iterations vs absolute error in the solution of Problem 2 using* $X_h^0 \times M_h^{1,m}$ *and* $X_h^0 \times M_h^1$ *discretizations and the methods PR and Newton.*
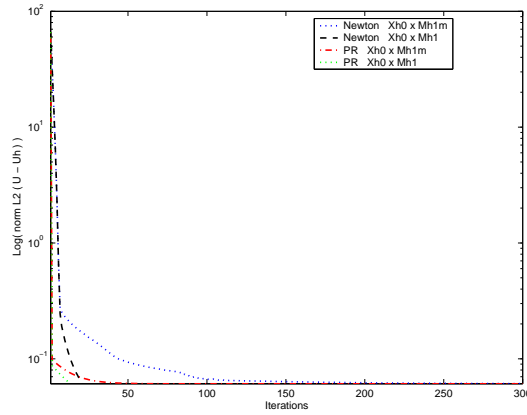

FIGURE 6.6. *Number of iterations vs absolute error in the solution of Problem 3 using* $X_h^0 \times M_h^{1,m}$ *and* $X_h^0 \times M_h^1$ *discretizations and the methods PR and Newton.*

oretically in [11], was corroborated. The results obtained through our test problems indicate that the PR iterative method is very attractive for numerically solving Darcy-Forchheimer's model with both discretizations. However, for the $X_h^0 \times M_h^1$ discretization, the CPU and memory requirements are lower and there is not much difference in the number of iterations compared with the $X_h^0 \times M_h^{1,m}$ discretization. For that reason, the $X_h^0 \times M_h^1$ discretization is a better choice.

In a future paper, we would like to study the convergence of velocity vector approximation using the PR method and the space discretization $X_h^0 \times M_h^1$, to propose other mixed finite elements, and to solve the nonlinear systems with other iterative methods of low computational cost. As for obtaining an accurate approximation for the pressure and low computational cost, it would be interesting to use a remark in [11] in which the solution of a Poisson equation for recovering a pressure approximation is proposed. We also would like to compare our results with those of other researchers in numerical simulations of flow models with a projection.

REFERENCES

[1] R. A. ADAMS, *Sobolev Spaces*, Academic Press, New York, 1975.

[2] M. I. S. AZZAM AND A. L. DULLIEN, *Flow rate-pressure gradient measurements in periodically nonuniform capillary tubes*, AIChE Journal, 19 (1973), pp. 22–229.

[3] G. S. BEAVERS AND E. M. SPARROW, *Non-Darcy flow through fibrous porous media*, Trans. ASME J. Appl. Mech., 36 (1969), pp. 711–714.

[4] L. S. BENNETHUM AND T. GIORGI, *Generalized Forchheimer equation for two-phase flow based on hybrid mixture theory*, Transp. Porous Media, 26 (1997), pp. 261–275.

[5] P. G. CIARLET, *The Finite Element Method for Elliptic Problems*, North-Holland, Amsterdam, 1978.

[6] M. CROUZEIX AND P. A. RAVIART, *Conforming and non-conforming finite element methods for solving the stationary Stokes problem*, RAIRO Anal. Numér., 7 (1973), pp. 33–76.

[7] J. DUPUIT, *Études Théoriques et Pratiques sur le Mouvement des Eaux*, Dunod, Paris, 1863.

[8] H. ELMAN, D. SILVESTER, AND A. WATHEN, *Finite Elements and Fast Iterative Solvers with applications in incompressible fluid dynamics*, Oxford University Press, Oxford, 2005.

[9] P. FABRIE, *Regularity of the solution of Darcy-Forchheimer's equation*, Nonlinear Anal., 13 (1989), pp. 1025–1049.

[10] P. FORCHHEIMER, *Wasserbewegung durch Boden*, Z. Ver. Deutsch. Ing., 45 (1901), pp. 1782–1788.

[11] V. GIRAULT AND M. F. WHEELER, *Numerical discretization of a Darcy-Forchheimer model*, Numer. Math., 110 (2008), pp. 161–198.

[12] A. GREENBAUM, *Iterative Methods for Solving Linear Systems*, SIAM, Philadelphia, 1997.

[13] E. ISAACSON AND H. B. KELLER, *Analysis of Numerical Methods*, Dover, Mineola, New York, 1994.

[14] R. JUMAH, F. A. BANAT AND F. ABU-AL-RUB, *Darcy-Forchheimer mixed convection heat and mass transfer in fluid saturated porous media*, Int. J. Numer. Meth. Heat Fluid Flow, 11 (2001), pp. 600–618.

[15] C. T. KELLEY, *Iterative Methods for Linear and Nonlinear Equations*, SIAM, Philadelphia, 1995.

[16] C. KIM AND J. E. PASCIAK, *A lowest order mixed finite element code for Forchheimer flow*, Technical Report, Texas A&M University, 1997.
Available at: http://www.math.tamu.edu/research/numerical_analysis/porous/

[17] C. KIM, J. E. PASCIAK, AND S. L. WEEKES, *A lowest order mixed finite element code for Forchheimer flow II*, Technical Report, Texas A&M University, 1997.
Available at: http://www.math.tamu.edu/research/numerical_analysis/porous/

[18] J. L. LIONS AND E. MAGENES, *Problémes aux Limites non Homogénes et Applications*, I, Dunod, Paris, 1968.

[19] G. I. MARCHUK, *Splitting and alternating direction methods*, in Handbook of Numerical Analysis, Volume I: Finite Difference Methods, P. G. Ciarlet and J. L. Lions, eds., North-Holland, Amsterdam, 1990.

[20] C. C. PAIGE AND M. A. SAUNDERS, *Solution of sparse indefinite systems of linear equations*, SIAM J. Numer. Anal., 11 (1974), pp. 197–209.

[21] D. W. PEACEMAN AND H. H. RACHFORD, *The numerical solution of parabolic and elliptic differential equations*, J. Soc. Indust. Appl. Math., 3 (1955), pp. 28–41.

[22] J. E. ROBERTS AND J.-M. THOMAS, *Mixed and hybrid methods*, in Handbook of Numerical Analysis, Volume II: Finite Element Methods, P. G. Ciarlet and J. L. Lions, eds., North-Holland, Amsterdam, 1991.

[23] Y. SAAD, *Iterative Methods for Linear Systems*, PWS, Boston, 1996.

[24] M. R. TEK, *Development of a generalized Darcy equation*, Trans. AIME, 210 (1957), pp. 376–377.

[25] J. W. THOMAS, *Numerical Partial Differential Equations*, Springer, New York, 1995.

[26] J. M. URQUIZA, D. N. DRI, A. GARON AND M. C. DELFOUR, *A numerical study of a primal mixed finite element approximations of a Darcy equations*, Commun. Numer. Methods Engng., 22 (2006), pp. 901–915.

[27] H. A. VAN DER VORST, *Iterative Krylov Methods for Large Linear Systems*, Cambridge University Press, Cambridge, 2003.

[28] J. C. WARD, *Turbulent flow in porous media*, J. Hydr. Div. ASCE, 90 (1964), pp. 1–12.

[29] D. M. YOUNG, *Iterative Solution of Large Linear Systems*, Dover, Mineola, New York, 2003.